Supporting Information

Split Locations and Secondary Structures of a DNAzyme Critical to Binding-Assembled Multicomponent Nucleic Acid Enzymes for Protein Detection

Yiren Cao, Hongquan Zhang*, and X. Chris Le*

Division of Analytical and Environmental Toxicology, Department of Laboratory Medicine and Pathology, Faculty of Medicine & Dentistry, University of Alberta, Edmonton, Alberta, Canada T6G 2G3

E-mail: hongquan@ualberta.ca and xc.le@ualberta.ca

Table of Contents

Table S1. Sequences of DNAzyme 10-23 and of 28 pairs of the subunits of MNAzymes for the study of the effect of different split locations and structures. '1hb' and 'b*2' form the four-arm structure. '1c' and 'c*2' form the three-arm structure. 'Pair 1' through to 'Pair 14' show 14 different split locations. Sequences in red are the intact or split catalytic core regions. Sequences in green and blue are the binding arms complementary to the substrate (FAM-1*2*, Table S2). Sequences in black are the hairpin structure, which is the fourth arm of the four-arm structure. Sequences in purple are the complementary regions for the assembly of the MNAzymes.

DNA name		**Sequence (5′ to 3′)**
DNAzyme 10-23		CA GTC AGA GGC TAG CTA CAA CGA GGT CCA TG
1hb	Pair 1	CAG TCA GA G GTG AG TTTTT CTC AC AGA CGT CAG CTC CA
	Pair 2	CAG TCA GA GG GTG AG TTTTT CTC AC AGA CGT CAG CTC CA
	Pair 3	CAG TCA GA GGC GTG AG TTTTT CTC AC AGA CGT CAG CTC CA
	Pair 4	CAG TCA GA GGC T GTG AG TTTTT CTC AC AGA CGT CAG CTC CA
	Pair 5	CAG TCA GA GGC TA GTG AG TTTTT CTC AC AGA CGT CAG CTC CA
	Pair 6	CAG TCA GA GGC TAG GTG AG TTTTT CTC AC AGA CGT CAG CTC CA
	Pair 7	CAG TCA GA GGC TAG C GTG AG TTTTT CTC AC AGA CGT CAG CTC CA
	Pair 8	CAG TCA GA GGC TAG CT GTG AG TTTTT CTC AC AGA CGT CAG CTC CA
	Pair 9	CAG TCA GA GGC TAG CTA GTG AG TTTTT CTC AC AGA CGT CAG CTC CA
	Pair 10	CAG TCA GA GGC TAG CTA C GTG AG TTTTT CTC AC AGA CGT CAG CTC CA
	Pair 11	CAG TCA GA GGC TAG CTA CA GTG AG TTTTT CTC AC AGA CGT CAG CTC CA
	Pair 12	CAG TCA GA GGC TAG CTA CAA GTG AG TTTTT CTC AC AGA CGT CAG CTC CA
	Pair 13	CAG TCA GA GGC TAG CTA CAA C GTG AG TTTTT CTC AC AGA CGT CAG CTC CA
	Pair 14	CAG TCA GA GGC TAG CTA CAA CG GTG AG TTTTT CTC AC AGA CGT CAG CTC CA

b*2	Pair 1	TGG AGC TGA CGT CT GC TAG CTA CAA CGA GGT CCA TG
	Pair 2	TGG AGC TGA CGT CT C TAG CTA CAA CGA GGT CCA TG
	Pair 3	TGG AGC TGA CGT CT TAG CTA CAA CGA GGT CCA TG
	Pair 4	TGG AGC TGA CGT CT AG CTA CAA CGA GGT CCA TG
	Pair 5	TGG AGC TGA CGT CT G CTA CAA CGA GGT CCA TG
	Pair 6	TGG AGC TGA CGT CT CTA CAA CGA GGT CCA TG
	Pair 7	TGG AGC TGA CGT CT TA CAA CGA GGT CCA TG
	Pair 8	TGG AGC TGA CGT CT A CAA CGA GGT CCA TG
	Pair 9	TGG AGC TGA CGT CT CAA CGA GGT CCA TG
	Pair 10	TGG AGC TGA CGT CT AA CGA GGT CCA TG
	Pair 11	TGG AGC TGA CGT CT A CGA GGT CCA TG
	Pair 12	TGG AGC TGA CGT CT CGA GGT CCA TG
	Pair 13	TGG AGC TGA CGT CT GA GGT CCA TG
	Pair 14	TGG AGC TGA CGT CT A GGT CCA TG
1c	Pair 1	CAG TCA GA G GGT GCA CGT CTC AG
	Pair 2	CAG TCA GA GG GGT GCA CGT CTC AG
	Pair 3	CAG TCA GA GGC GGT GCA CGT CTC AG
	Pair 4	CAG TCA GA GGC T GGT GCA CGT CTC AG
	Pair 5	CAG TCA GA GGC TA GGT GCA CGT CTC AG
	Pair 6	CAG TCA GA GGC TAG GGT GCA CGT CTC AG
	Pair 7	CAG TCA GA GGC TAG C GGT GCA CGT CTC AG
	Pair 8	CAG TCA GA GGC TAG CT GGT GCA CGT CTC AG
	Pair 9	CAG TCA GA GGC TAG CTA GGT GCA CGT CTC AG
	Pair 10	CAG TCA GA GGC TAG CTA C GGT GCA CGT CTC AG
	Pair 11	CAG TCA GA GGC TAG CTA CA GGT GCA CGT CTC AG
	Pair 12	CAG TCA GA GGC TAG CTA CAA GGT GCA CGT CTC AG
	Pair 13	CAG TCA GA GGC TAG CTA CAA C GGT GCA CGT CTC AG
	Pair 14	CAG TCA GA GGC TAG CTA CAA CG GGT GCA CGT CTC AG
c*2	Pair 1	CTG AGA CGT GCA CC GC TAG CTA CAA CGA GGT CCA TG
	Pair 2	CTG AGA CGT GCA CC C TAG CTA CAA CGA GGT CCA TG
	Pair 3	CTG AGA CGT GCA CC TAG CTA CAA CGA GGT CCA TG
	Pair 4	CTG AGA CGT GCA CC AG CTA CAA CGA GGT CCA TG
	Pair 5	CTG AGA CGT GCA CC G CTA CAA CGA GGT CCA TG
	Pair 6	CTG AGA CGT GCA CC CTA CAA CGA GGT CCA TG
	Pair 7	CTG AGA CGT GCA CC TA CAA CGA GGT CCA TG
	Pair 8	CTG AGA CGT GCA CC A CAA CGA GGT CCA TG
	Pair 9	CTG AGA CGT GCA CC CAA CGA GGT CCA TG
	Pair 10	CTG AGA CGT GCA CC AA CGA GGT CCA TG
	Pair 11	CTG AGA CGT GCA CC A CGA GGT CCA TG
	Pair 12	CTG AGA CGT GCA CC CGA GGT CCA TG
	Pair 13	CTG AGA CGT GCA CC GA GGT CCA TG
	Pair 14	CTG AGA CGT GCA CC A GGT CCA TG

Table S2. Sequences of the substrate, DNA subunits, spacer, and aptamer used for the detection of proteins. 1HB and B*2 are two biotinylated DNA subunits that bind to streptavidin. 1HB-15 and 29-B*2 are aptamer-conjugated DNA subunits recognizing thrombin. Sequences in *italics* are aptamer sequences (15-mer and 29-mer) binding to thrombin. Underlined sequences are designed to form the double-stranded spacers after hybridization with Poly-A spacer. FAM-1*2* is the substrate labeled with thiol group at the 5′-end and fluorescein amidite (FAM) at the 3′-end. Ribonucleotides in **bold** indicate the cleavage site of the substrate.

DNA name	**Sequence (5′ to 3′)**
1HB	CAG TCA GA GGC TAG C GTG AG TTTTT CTC AC AGT GTT C AT TTT TTT TTT TTT TTT TTT-Biotin
B*2	Biotin-TTT TTT TTT TTT TTT TTT TA GAA CAC T TAC AAC GA GG TCC ATG
1HB-15	CAG TCA GA GGC TAG C GTG AG TTTTT CTC AC AGT GTT C A T TTT TTT TTT TTT TTT *GGT TGG TGT GGT TGG*
29-B*2	*AGT CCG TGG TAG GGC AGG TTG GGG TGA CT* TTT TTT TTT TTT TTT T A GAA CAC T TAC AAC GA GG TCC ATG
Poly-A spacer	AAA AAA AAA AAA AAA A
FAM-1*2*	HS-TTT TTT TTT TTT CA TGG ACC **rG U** CTG ACT G T-FAM

Table S3. Multiple turnover number ($k_{obs.m}$, min^{-1}) of the intact DNAzyme 10-23 and of 28 MNAzymes designed to contain two secondary structures and assembled from subunits split at 14 locations. The symbol / denotes no detectable activity.

	$k_{obs.m}$ (min^{-1})	
DNAzyme 10-23	1.3	
split location	**four-arm structure**	**three-arm structure**
G_1/G_2	3.8×10^{-1}	/
G_2/C_3	2.1×10^{-1}	/
C_3/T_4	/	/
T_4/A_5	3.0×10^{-3}	/
A_5/G_6	6.7×10^{-2}	/
G_6/C_7	3.7×10^{-3}	/
C_7/T_8	5.3×10^{-1}	3.3×10^{-1}
T_8/A_9	3.3×10^{-2}	2.1×10^{-1}
A_9/C_{10}	3.7×10^{-1}	6.2×10^{-3}
C_{10}/A_{11}	8.3×10^{-3}	/
A_{11}/A_{12}	1.7×10^{-2}	1.5×10^{-3}
A_{12}/C_{13}	4.3×10^{-1}	1.1×10^{-3}
C_{13}/G_{14}	2.0×10^{-1}	/
G_{14}/A_{15}	3.3×10^{-2}	/

Table S4. Limits of detection of reported homogeneous assays for the detection of streptavidin and thrombin.

Target protein	Detection	Signal amplification	Detection limit	Ref.
thrombin	fluorescent	DNAzyme cleavage reaction	36 pM	this work
thrombin	colorimetric	G-quadruplex DNAzyme catalytic beacon	20.5 nM	1
thrombin	fluorescent	nicking enzyme amplification	40 pM	2
thrombin	fluorescent	no amplification	50 pM	3
thrombin	fluorescent	G-quadruplex DNAzyme catalytic beacon	1 pM	4
thrombin	colorimetric	nanoparticle-based catalytic beacon	190 pM	5
streptavidin	fluorescent	DNAzyme cleavage reaction	1.3 pM	this work
streptavidin	fluorescent	catalytic DNA circuit	10 pM	6
streptavidin	fluorescent	DNAzyme cleavage reaction	0.5 pM	7

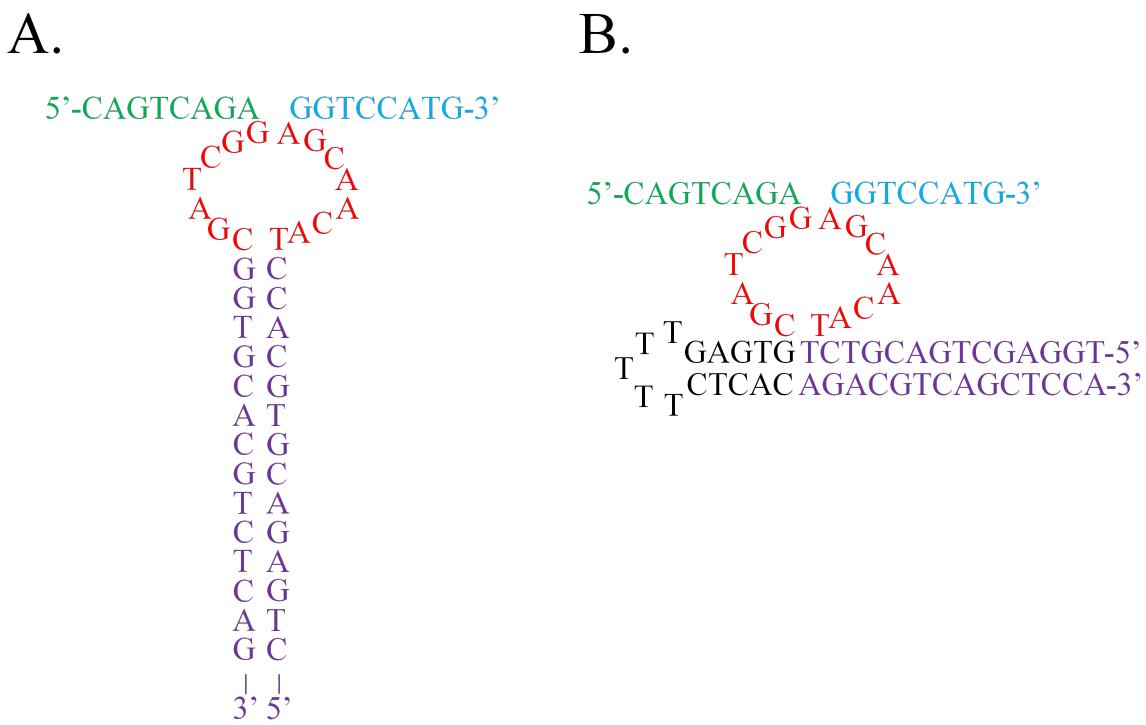

Figure S1. Schematic showing the three-arm structure (A) and the four-arm structure (B) of the MNAzymes. The green and blue sequences are the binding arms, the red sequences are the split catalytic core regions, and the purple sequences are the complementary regions of MNAzymes.

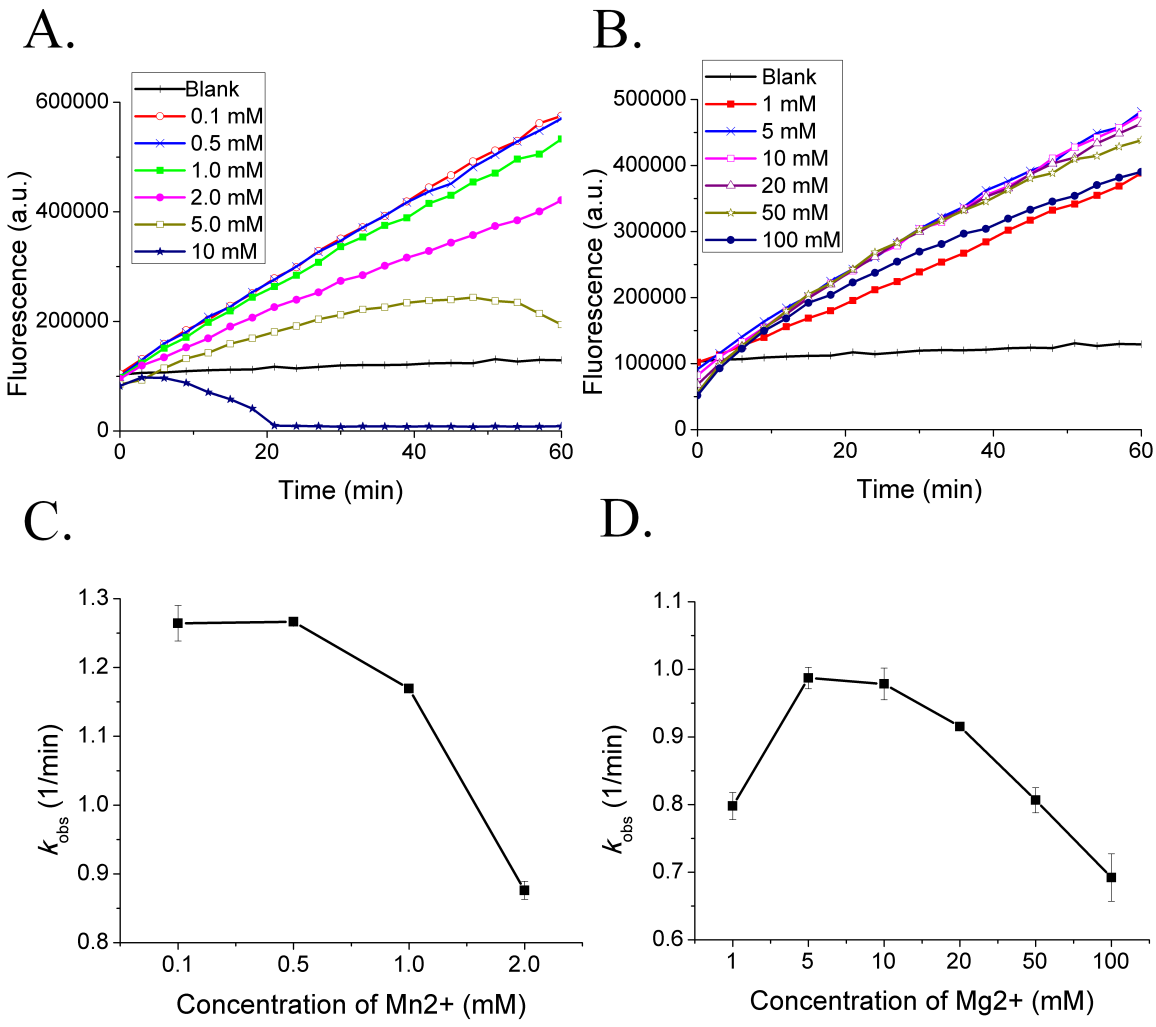

Figure S2. Optimization of the cofactor conditions. Each sample contained 0.2 nM DNAzyme 10-23, 0.2 nM substrate-conjugated AuNPs (estimated loading amount of 400 substrates per AuNP), 200 mM NaCl, 20 mM Tris-acetate (pH=8.5), and varying concentrations of $MnCl_2$ or $MgCl_2$. (A) Real-time monitoring of fluorescence intensities over 60 min for samples under the 0.1−10 mM $MnCl_2$ cofactor conditions. (B) Real-time monitoring of fluorescence intensities over 60 min for samples under the 1−100 mM $MgCl_2$ cofactor conditions. (C) $k_{obs.m}$ of DNAzyme in the presence of 0.1−2 mM $MnCl_2$. (D) $k_{obs,m}$ of DNAzyme in the presence of 1−100 mM $MgCl_2$. Too high a concentration of Mn^{2+} (> 5 mM) led to the precipitation and dramatic decrease in the fluorescence intensity in the buffer at pH 8.5.

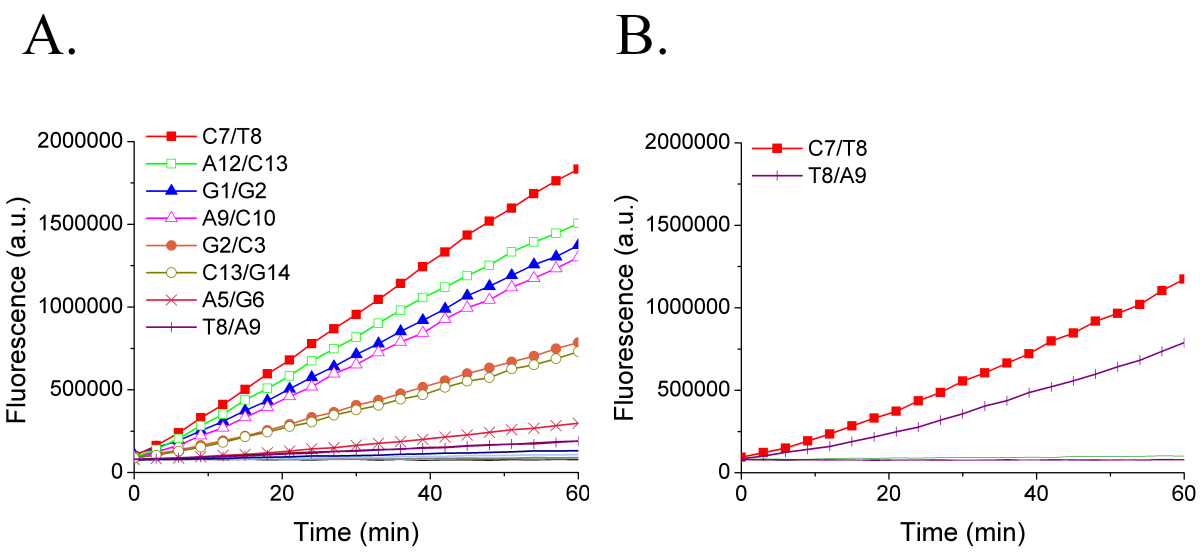

Figure S3. Fluorescence intensities generated by the catalytic cleavage of the substrates by various MNAzymes. The MNAzymes of the four-arm structure (A) and three-arm structure (B) were assembled from the subunits split at different locations of DNAzyme 10-23. Each sample contained 2 nM MNAzymes, 0.2 nM substrate-conjugated AuNPs (equivalent to 80 nM substrate), 200 mM NaCl, 20 mM Tris-acetate (pH=8.5), 0.5 mM $MnCl_2$ and 10 mM $MgCl_2$. (A) Real-time monitoring of fluorescence intensities (arbitrary unit) over 60 min for the MNAzymes with the four-arm structure assembled from two subunits at eight specified split locations. (B) Real-time monitoring of fluorescence intensities over 60 min for the MNAzymes with the three-arm structure assembled from two subunits at two specified split locations. The MNAzymes assembled from two subunits at other split locations did not show observable activity and their cleavage curves were included but not labeled in the figure. 'C7/T8' indicates the split location is between C_7 and T_8 in the catalytic core region.

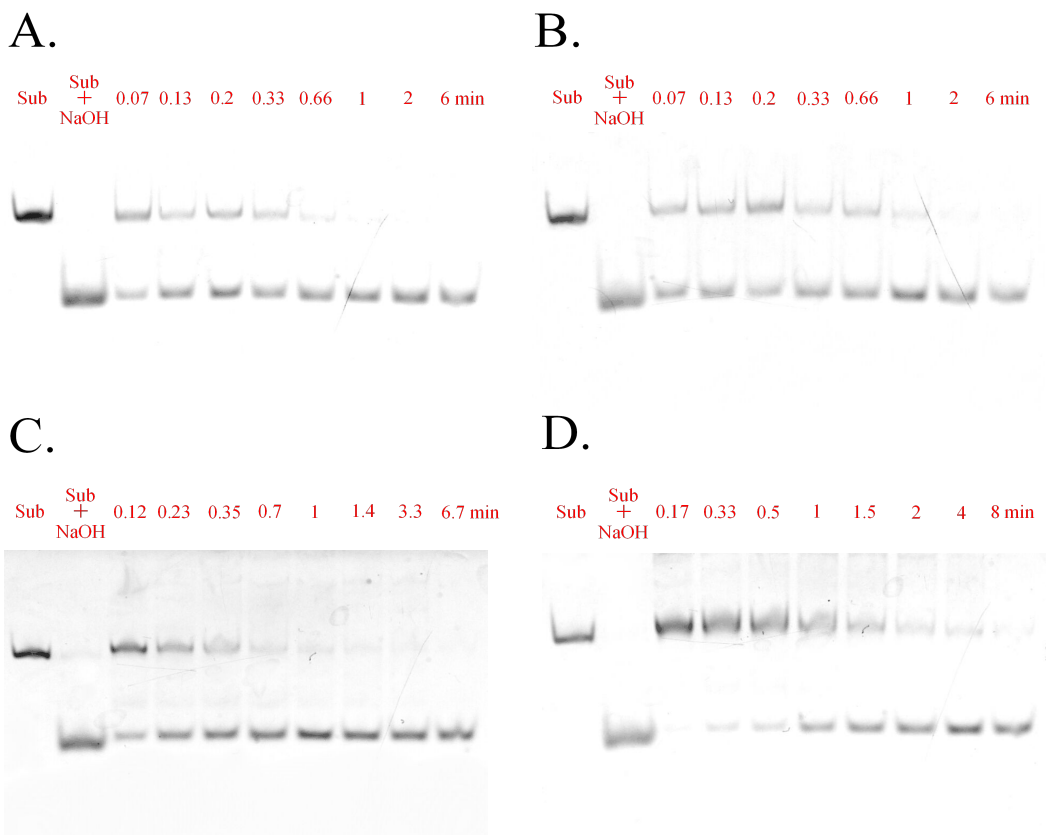

Figure S4. Gel images showing the single turnover cleavage by the intact DNAzyme 10-23 and the assembled MNAzyme of the C_7/T_8 split location (Figure S1A). (A) Cleavage by the intact DNAzyme 10-23 in the presence of 2 mM Mn^{2+}. (B) Cleavage by the MNAzyme in the presence of 2 mM Mn^{2+} (C) Cleavage by the intact DNAzyme 10-23 in the presence of 10 mM Mg^{2+}. (D) Cleavage by the MNAzyme in the presence of 10 mM Mg^{2+}. The DNAzyme or MNAzymes (4 μM) was mixed with 2 μM FAM-1*2* (Table S2) in Tris-EDTA (pH=8.0). After 10 min incubation at room temperature, 2 mM Mn^{2+} or 10 mM Mg^{2+} was added to initiate the reaction. From designated time points after the addition of cofactor Mn^{2+} or Mg^{2+}, 10 μL reaction solution was sampled and mixed with 10 μL 50 mM EDTA to terminate the reaction. Then, the mixture was loaded onto a 14% native PAGE gel for analysis at 100 V for 60 min. The first lane and second lane in the gel images were the substrate in buffer (negative control) and the substrate hydrolyzed by NaOH (positive control), respectively.

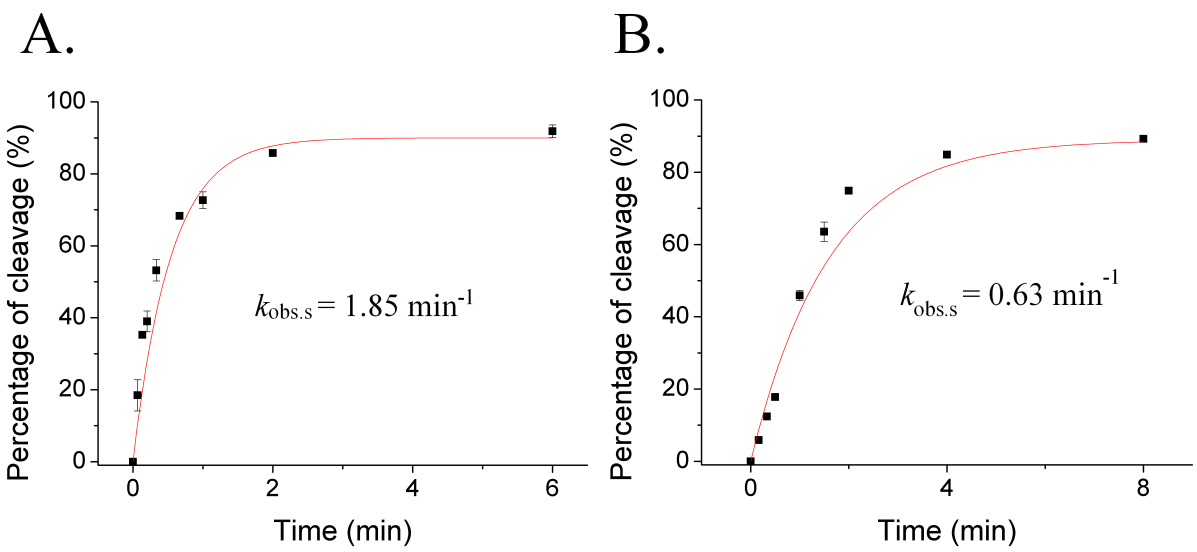

Figure S5. Cleavage curves (percentage of cleavage over time) used to determine the single turnover number ($k_{obs.s}$, min^{-1}) of the intact DNAzyme 10-23 (A) and the MNAzyme assembled from subunits of the C_7/T_8 split location (B). Mg^{2+} (10 mM) was used as the cofactor. The percentage of cleavage was obtained from the results of the band intensity of gel images in Figure S4. (A) Percentage of 2 μM substrate cleaved by 4 μM of the intact DNAzyme 10-23. Curve fitting showing the $k_{obs,s}$ of the DNAzyme. (B) Percentage of 2 μM substrate cleaved by 4 μM of the MNAzyme assembled from subunits of the C_7/T_8 split location. Curve fitting showing the $k_{obs,s}$ of the MNAzymes.

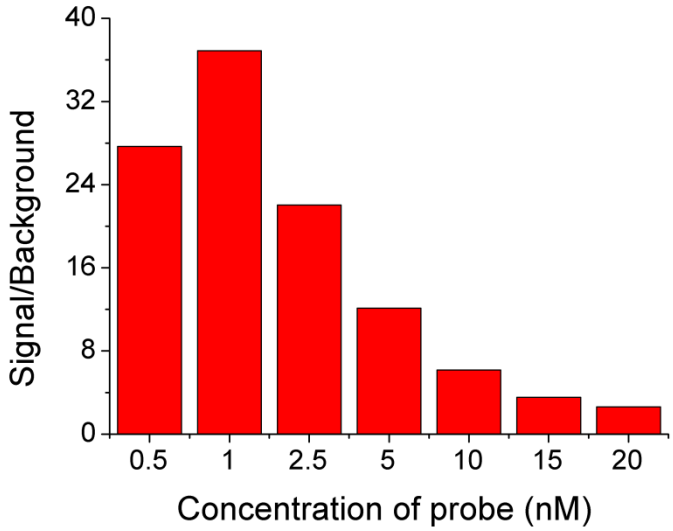

Figure S6. Optimization of the concentrations of the split subunits, 1HB and B*2 (Table S2), for the detection of streptavidin. Each sample contained 0.2 nM substrate-conjugated AuNPs, 200 mM NaCl, 20 mM Tris-acetate (pH=8.5), 0.5 mM $MnCl_2$, and 200 pM streptavidin bound with 0.5−20 nM 1HB and B*2. Streptavidin was incubated with two subunits for 15 min at room temperature. The fluorescence intensities of duplicate samples and blanks at 1 h were used to calculate the signal-to-background ratio.

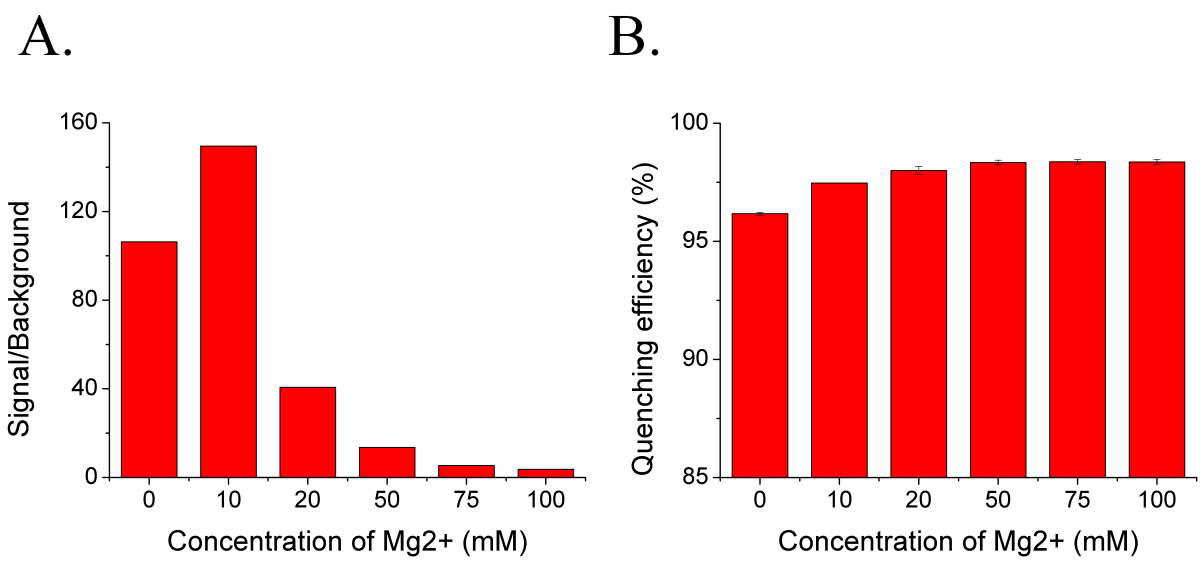

Figure S7. Optimization of Mg^{2+} concentration for the detection of streptavidin. (A) Relationship between the concentration of Mg^{2+} and the signal-to-background ratio. Each sample contained 0.2 nM substrate-conjugated AuNPs, 200 mM NaCl, 20 mM Tris-acetate (pH=8.5), 0.5 mM $MnCl_2$, 200 pM of streptavidin bound with 1 nM of DNA subunits (1HB and B*2), and 0−100 mM Mg^{2+}. The fluorescence intensities of duplicate samples and blanks at 1 h were used to calculate the signal-to-background ratio. (B) Improvement of the quenching efficiency of AuNP by Mg^{2+}. Quenching efficiency (%) = fluorescence value of 0.2 nM substrate-conjugated AuNPs / fluorescence value of 0.2 nM conjugates incubated with 2-mercaptoethanol overnight. The overnight incubation of AuNPs with 2-mercaptoethanol was to completely release all the conjugated substrates.

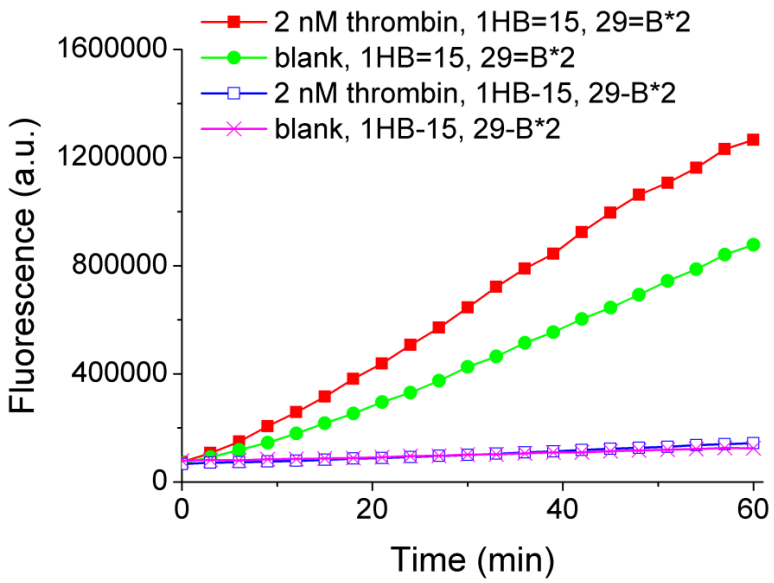

Figure S8. A comparison between the double-stranded and single-stranded spacers of the subunits for thrombin detection. 1HB=15 and 29=B*2 are DNA subunits of the double-stranded spacer formed by annealing poly-A and 1HB-15 (or 29-B*2, Table S2). Each sample contained 0.2 nM substrate-conjugated AuNPs, 200 mM NaCl, 20 mM Tris-acetate (pH=8.5), 0.5 mM $MnCl_2$, 10 nM of two DNA subunits, and 10 mM Mg^{2+}. Thrombin was incubated with DNA subunits for 60 min at room temperature. No fluorescence increase was observed for the blank and the sample containing 2 nM thrombin when subunits of single-stranded spacer, 1HB-15 and 29-B*2, were used. This result suggests that the aptamer sequence can interact with the sequences of the partial DNAzyme, impairing the desired assembly of the two subunits. Introducing a double-stranded spacer reduced the intramolecular interaction between the aptamer and the partial DNAzyme, which facilitates the binding-induced assembly of the two subunits. The relatively high background from the blank (green curve) was due to a higher concentration (10 nM) of the subunits used in this experiment, which increased the chances of target-independent assembly of the subunits. When the concentration of the subunits was reduced to 2 nM, the background was significantly decreased as shown in Figure 6.

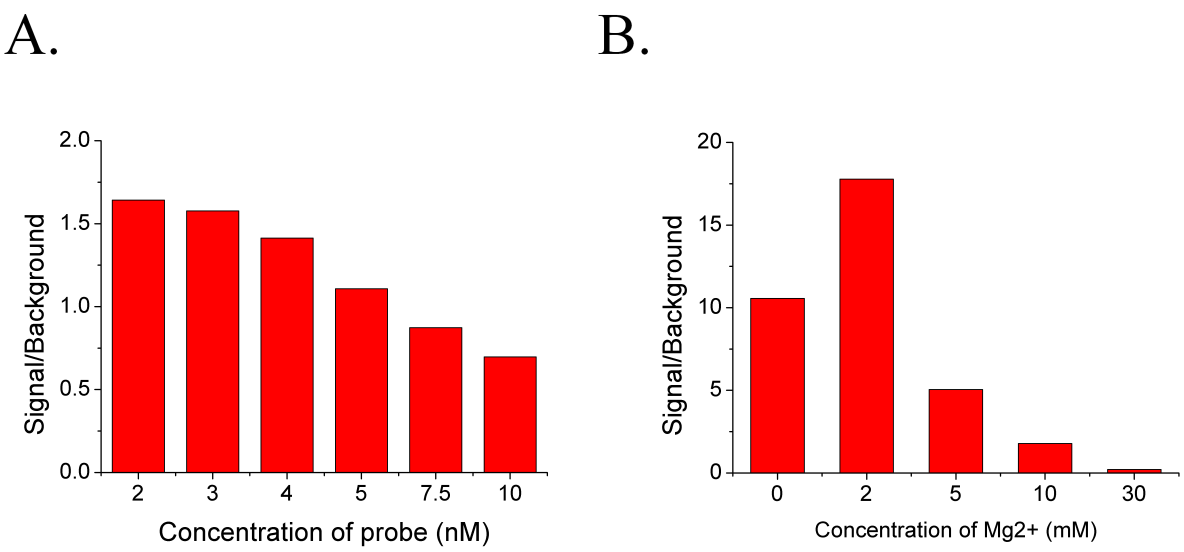

Figure S9. Optimization of the concentrations of the aptamer-conjugated subunits 1HB=15 and 29=B*2 (A) and concentrations of Mg^{2+} (B) for the detection of thrombin. Thrombin was incubated with the subunits for 60 min at room temperature. The fluorescence values of duplicate samples and blanks at 1 h were used to calculate the signal-to-background ratio. (A) Each sample contained 0.2 nM substrate-conjugated AuNPs, 200 mM NaCl, 20 mM Tris-acetate (pH=8.5), 0.5 mM $MnCl_2$, 10 mM $MgCl_2$, and 2 nM thrombin bound with 2−10 nM of two subunits. (B) each sample contained 0.2 nM substrate-conjugated AuNPs, 200 mM NaCl, 20 mM Tris-acetate (pH=8.5), 0.5 mM $MnCl_2$, 2 nM thrombin bound with 2 nM subunits, and 0−30 mM $MgCl_2$.

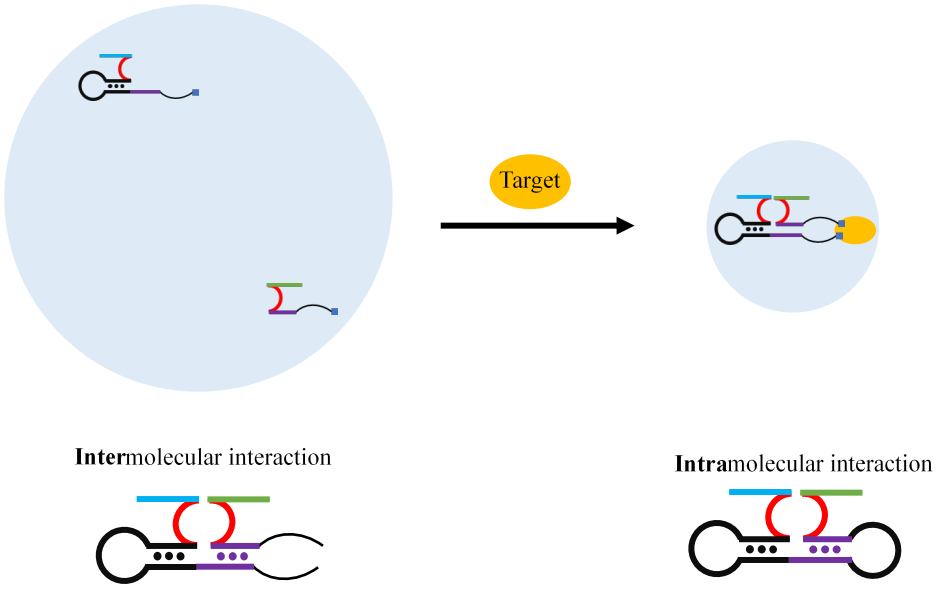

Figure S10. Schematic illustration of binding-induced assembly, which increases the local effective concentrations of the interacting subunits, changes the nature of interaction from intermolecular to intramolecular, and increases the melting temperature (T_m) of the hybrid. Two approaches were used to estimate the T_m of the hybrid between two 7-base complementary sequences. Under the conditions of 1 nM subunits, 200 nM Na^+, and 10 mM Mg^{2+}, the hybrid between the two subunits containing a complementary sequence of 7 base pairs had an estimated T_m of 0.5 °C (IDT oligo analyzer 3.1). Binding of the two subunits to the same target protein molecule brought the two subunits into the same molecule. With an approximate molecular size of 20 nm in diameter, the estimated molecular volume was 4.2 zL. One molecule in 4.2 zL was equivalent to a local effective concentration to 400 μM.[8] Under the conditions of 400 μM subunits, 200 nM Na^+, and 10 mM Mg^{2+}, the estimated T_m of the hybrid between the two subunits containing the complementary sequence of 7 base pairs was 48.6 °C. The second approach for estimating the T_m of the intramolecular hybridization was to use a hairpin structure, in which two 7-base complementary sequences acted as the stem and a 50-nt polyT acted as the loop to simulate the spatial distance of the spacer sequence and the ternary complex molecule between two probes and one protein molecule. The T_m of the hybrid formed with the stem region of this hairpin was estimated to be 45.3 °C (1 nM hairpin, 200 nM Na^+, 10 mM Mg^{2+}). The estimated T_m represented the stability of the hybrid of two 7-base complementary sequences after the ternary complex was formed.

References

(1) Zhang, L.; Zhu, J.; Li, T.; Wang, E. *Anal. Chem.* **2011**, *83*, 8871–8876.

(2) Xue, L.; Zhou, X.; Xing, D. *Chem. Commun.* **2010**, *46*, 7373–7375.

(3) Heyduk, E.; Heyduk, T. *Anal. Chem.* **2005**, *77*, 1147–1156.

(4) Zhang, Y.; Li, B.; Jin, Y. *Analyst* **2011**, *136*, 3268–3273.

(5) Gao, L.; Zhuang, J.; Nie, L.; Zhang, J.; Zhang, Y.; Gu, N.; Wang, T.; Feng, J.; Yang, D.; Perrett, S. *Nat. Nanotech.* **2007**, *2*, 577–583.

(6) Li, F.; Zhang, H.; Wang, Z.; Li, X.; Li, X.-F.; Le, X. C. *J. Am. Chem. Soc.* **2013**, *135*, 2443–2446.

(7) Zhang, H.; Lai, M.; Zuehlke, A.; Peng, H.; Li, X. F.; Le, X. C. *Angew. Chem. Int. Ed.* **2015**, *127*, 14534–14538.

(8) Zhang, H.; Li, F.; Dever, B.; Wang, C.; Li, X. F.; Le, X. C. *Angew. Chem. Int. Ed.* **2013**, *52*, 10698–10705.